Damping of collective states in an extended random-phase approximation with ground-state correlations

Mitsuru Tohyama
Kyorin University School of Medicine, Mitaka, Tokyo 181-8611, Japan
(Received 12 January 2007; published 24 April 2007)

Applications of an extended version of the Hartree-Fock theory and the random-phase approximation derived from the time-dependent density-matrix theory (TDDM) are presented. In this TDDM-based theory, the ground state is given as a stationary solution of the TDDM equations and the excited states are calculated using the small-amplitude limit of TDDM. The first application presented is an extended Lipkin model in which an interaction term describing a particle scattering is added to the original Hamiltonian so that the damping of a collective state is taken into account. It is found that the TDDM-based theory well reproduces the ground state and excited states of the extended Lipkin model. The quadrupole excitation of the oxygen isotopes ^{16,20,22}O is also studied as realistic applications of the TDDM-based theory. It is found that large fragmentation of the giant quadrupole resonance in ^{16}O is reproduced, and it is pointed out that the effects of ground-state correlations are quite important for fragmentation. It is also found that the quadrupole states in neutron-rich oxygen isotopes have small spreading widths.

DOI: 10.1103/PhysRevC.75.044310 PACS number(s): 21.60.Jz, 21.10.Re, 24.30.Cz, 27.20.+n

I. INTRODUCTION

The random phase approximation (RPA) based on the Hartree-Fock (HF) ground state and the quasiparticle RPA (QRPA) based on the Hartree-Fock-Bogoliubov (HFB) ground state have extensively been used as standard microscopic theories to study collective excitation in stable nuclei [1] and in unstable nuclei [2–5]. However, the RPA and QRA which correspond to the small-amplitude limit of the time-dependent mean-field theories, that is, the time-dependent HF theory (TDHF) and the time-dependent HFB theory, respectively, do not include higher-order correlations that cause the damping of collective states. For a realistic description of nuclear collective excitation, therefore, we must go beyond the mean-field theories [6]. The time-dependent density-matrix theory (TDDM) [7,8] which incorporates the effects of nucleon-nucleon collisions into TDHF is one of such extended mean-field theories. It was pointed out [9] that the small-amplitude limit of TDDM (STDDM) is an extended version of RPA which includes the effects of two-body correlations in both the ground and excited states. However, this TDDM-based approach (STDDM based on the TDDM ground state) has become applicable only recently after a somewhat puzzling problem [10] of finding the ground state in TDDM was solved by introducing the gradient method [11]. We have applied the TDDM-based approach to the Lipkin model [12] and to the quadrupole excitation in neutron-rich oxygen isotopes [11,13]. Although the obtained results were encouraging, whether the TDDM-based approach is appropriate for the description of the damping of collective states has not been determined because of the limitations in these applications: the Lipkin model Hamiltonian [14] used in Ref. [12] does not have interaction terms causing the damping of a collective state, and the number of single-particle states used for the quadrupole excitation in oxygen isotopes [13] was not sufficient to study the damping of giant quadrupole resonances (GQRs). In this paper, we present further applications of the TDDM-based approach and show that our approach properly describes the damping properties of collective states. First we show the results for an extended Lipkin model in which an interaction term describing particle scattering is added to the original Hamiltonian so that the damping of a collective state is taken into account. Then we present the quadrupole excitation including GQR in the oxygen isotopes ^{16,20,22}O calculated using much larger single-particle space than used in Ref. [11,13]. We point out that the damping properties of the quadrupole states in the neutron-rich isotopes differ from those in ^{16}O. The paper is organized as follows. The formulation of the TDDM-based approach is presented in Sec. II. Results for the extended Lipkin model and the oxygen isotopes are shown in Sec. III, and Sec. IV is devoted to the summary.

II. FORMULATION

A. Ground state in TDDM

In TDDM, the ground state $|\Phi_0\rangle$ is specified by the occupation matrix $n_{\alpha\alpha'}$ and the two-body correlation matrix $C_{\alpha\beta\alpha'\beta'}$, that is,

$$n_{\alpha\alpha'} = \langle\Phi_0|a^+_{\alpha'}a_\alpha|\Phi_0\rangle, \quad (1)$$

$$C_{\alpha\beta\alpha'\beta'} = \langle\Phi_0|a^+_{\alpha'}a^+_{\beta'}a_\beta a_\alpha|\Phi_0\rangle - n_{\alpha\alpha'}n_{\beta\beta'} + n_{\alpha\beta'}n_{\beta\alpha'}, \quad (2)$$

where $a_\alpha(a^+_\alpha)$ is the annihilation (creation) operator of a nucleon at single-particle state α. The matrices $n_{\alpha\alpha'}$ and $C_{\alpha\beta\alpha'\beta'}$ are determined by the stationary condition of the TDDM equations, which is expressed by

$$F_1(\alpha\alpha') = \langle\Phi_0|[a^+_{\alpha'}a_\alpha, H]|\Phi_0\rangle = 0, \quad (3)$$

$$F_2(\alpha\beta\alpha'\beta') = \langle\Phi_0|[a^+_{\alpha'}a^+_{\beta'}a_\beta a_\alpha, H]|\Phi_0\rangle = 0, \quad (4)$$

where H is the total Hamiltonian. Equations (3) and (4) are explicitly given in Ref. [11], where the eigenstates of a mean-field Hamiltonian h are used as single-particle states ϕ_α. To obtain the ground state in TDDM means that all quantities,

$n_{\alpha\alpha'}$, $C_{\alpha\beta\alpha'\beta'}$ and ϕ_α, are determined under the conditions (3) and (4). It was found that this difficult task can be achieved using the gradient method [11]. Starting from a simple ground state such as the HF ground state, where $n_{\alpha\alpha'}$ and $C_{\alpha\beta\alpha'\beta'}$ are known, we iterate

$$\begin{pmatrix} n(N+1) \\ C(N+1) \end{pmatrix} = \begin{pmatrix} n(N) \\ C(N) \end{pmatrix} - \alpha \begin{pmatrix} a & c \\ b & d \end{pmatrix}^{-1} \begin{pmatrix} F_1(N) \\ F_2(N) \end{pmatrix} \quad (5)$$

until convergence is achieved. Here, $n(N)$, $C(N)$, $F_1(N)$, and $F_2(N)$ imply $n_{\alpha\alpha'}$, $C_{\alpha\beta\alpha'\beta'}$, $F_1(\alpha\alpha')$, and $F_2(\alpha\beta\alpha'\beta')$ at the Nth iteration step. Equation (5) is coupled to $h\phi_\alpha = \epsilon_\alpha\phi_\alpha$ because h depends on $n_{\alpha\alpha'}$. The matrix elements a, b, c, and d are given as the functional derivatives of F_1 and F_2: $a = \delta F_1/\delta n$, $b = \delta F_1/\delta C$, $c = \delta F_2/\delta n$, and $d = \delta F_2/\delta C$. These matrices are identical to the matrix elements of the STDDM equation [11]. We show them explicitly in the Appendix. A small parameter α is introduced to control the convergence process.

B. Small-amplitude limit of TDDM

The equations of STDDM are derived by linearizing the TDDM equations with respect to the deviations of the one- and two-body density matrices from their ground-state values [9]. The STDDM equations consist of the one-body transition amplitude $x^\mu_{\alpha\alpha'} = \langle\Phi_0|a^+_{\alpha'}a_\alpha|\Phi_\mu\rangle$ and the two-body transition amplitude $X^\mu_{\alpha\beta\alpha'\beta'} = \langle\Phi_0|a^+_{\alpha'}a^+_{\beta'}a_\beta a_\alpha|\Phi_\mu\rangle$, where $|\Phi_\mu\rangle$ is an excited state with excitation energy ω_μ. The equations in STDDM can be written in matrix form [15] as

$$\begin{pmatrix} a & c \\ b & d \end{pmatrix} \begin{pmatrix} x^\mu \\ X^\mu \end{pmatrix} = \omega_\mu \begin{pmatrix} x^\mu \\ X^\mu \end{pmatrix}, \quad (6)$$

where the matrix elements on the left-hand side are the same as those on the right-hand side of Eq. (5). The strength function $S(E)$ for an excitation operator $\hat{Q}$

$$S(E) = \sum_{\omega_\mu>0} |\langle\Phi_\mu|\hat{Q}|\Phi_0\rangle|^2\delta(E-\omega_\mu) \quad (7)$$

is calculated using the solution of Eq. (6). The detailed expression of $S(E)$ in terms of $x^\mu_{\alpha\alpha'}$ and $X^\mu_{\alpha\beta\alpha'\beta'}$ is given in Ref. [15]. Matrices a and d contain $n_{\alpha\alpha'}$, and matrix b has both $n_{\alpha\alpha'}$ and $C_{\alpha\beta\alpha'\beta'}$ (see Appendix). Thus, various effects of ground-state correlations—which may be classified as the self-energy contributions, the modification of particle-hole (p-h) interactions, and the vertex corrections [16]—are included in Eq. (6). The omission of ground-state correlations reduces STDDM to the second RPA [6], which has been extensively used to study the damping properties of giant resonances.

III. APPLICATIONS

A. Extended Lipkin model

The Lipkin model [14] describes an N-fermion system with two N-fold degenerate levels with energies $\epsilon/2$ and $-\epsilon/2$, respectively. The upper and lower levels are labeled by quantum numbers p and $-p$, respectively, with $p = 1, 2, \ldots, N$. We consider the Hamiltonian

$$H = \epsilon J_z + \frac{V}{2}(J_+^2 + J_-^2) + \frac{U}{2}[J_z(J_+ + J_-) + (J_+ + J_-)J_z], \quad (8)$$

where an additional interaction term proportional to U is introduced. The operators are given as

$$J_z = \frac{1}{2}\sum_{p=1}^{N}(a_p^+ a_p - a_{-p}{}^+ a_{-p}), \quad (9)$$

$$J_+ = J_-^+ = \sum_{p=1}^{N} a_p^+ a_{-p}. \quad (10)$$

The V term describes the 2p-2h excitation and deexcitation as shown in Fig. 1(a), while the U term allows a scattering of a particle (hole) state to a 2p-1h (2h-1p) state [Fig. 1(b)]. Due to the U term, two effects which are not included in the usual Lipkin model are introduced: One is the effect of a mean-field potential which always mixes the lower and upper levels as depicted in Fig. 2(a); the other is the damping of a phonon state [Fig. 2(b)], where a p-h state couples to a 2p-2h state. Therefore, this extended version of the Lipkin model is relevant to testing theoretical models designed for the damping of collective states. Similar extended versions of the Lipkin model Hamiltonian have been used in Refs. [17,18].

Using an $N = 4$ system as an example, we solve Eq. (5) for the ground states and Eq. (6) for the excited states. To solve these equations, we use the original single-particle basis

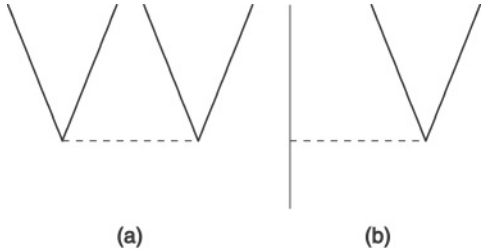

FIG. 1. (a) Two-particle–two-hole excitation described by the V term. (b) Scattering of a particle or hole state given by the U term in the extended Lipkin model. Dashed line denotes the interaction; solid lines, either particle states or hole states.

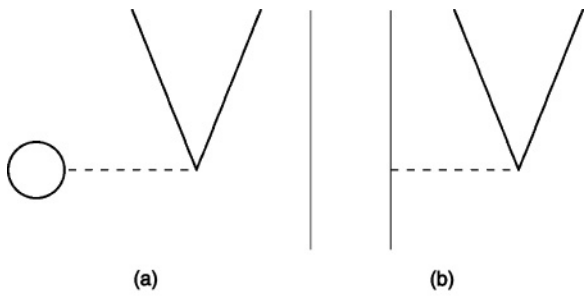

FIG. 2. Extended Lipkin model describing the effects of (a) a mean-field potential and (b) damping of a phonon state. Dashed line denotes the interaction; solid lines, either particle states or hole states.

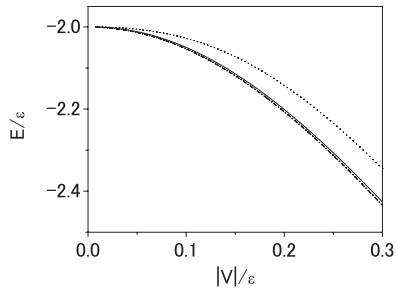

FIG. 3. Ground-state energy E/ϵ as a function of $|V|/\epsilon$ for $N = 4$ and $U = V/2$. Solid, dotted, and dot-dashed lines depict the TDDM results, HF results, and exact solutions, respectively.

specified by p and $-p$, whereas the HF basis is used for RPA and SRPA calculations. First we present the results for the ground states. We fix ϵ at 2 and change V for two cases, $U = V/2$ and $U = V$. The case of $U = 0$ was reported in our previous work [12]. The ground-state energies obtained in TDDM (solid line) for various interaction strength $|V|$ are shown in Figs. 3 and 4 in comparison with the exact and HF ones. The results in TDDM are very close to the exact ones in both cases with different relative strength of $|U|$. With increasing U (from $V/2$ to V), the results in HF become closer to the exact ones and two-body correlations become less important. This is because the spacing between the two single-particle states becomes larger with increasing U. This feature of the extended Lipkin model has been pointed out in Ref. [18].

Now we show the results for one-phonon states for $U = V/2$ (Fig. 5) and $U = V$ (Fig. 6) calculated at $V/\epsilon = -0.3$. The excitation operator used is $\hat{Q} = J_+ + J_- + J_z$. The solid lines show the strength functions in STDDM. The strength functions for the exact solution (dot-dashed line) and the solutions obtained in RPA (dotted line) and SRPA (dashed line) are also drawn for comparison. To facilitate easy comparison among the various calculations, we smoothed the strength functions with an artificial width (full width at half maximum) $\Gamma_{\mathrm{FWHM}}/\epsilon = 0.125$. RPA always gives a single state.

The one-phonon states in SRPA are split into two states. The first and second excited states in SRPA mainly consist of 1p-1h configurations and 2p-2h configurations with respect to the HF ground state, respectively.

STDDM gives fragmentation of strength into three states. In the case of $U = V/2$, the transition strength of the third exited state at $E/\epsilon = 3.1$ is too small to be seen in the scale of

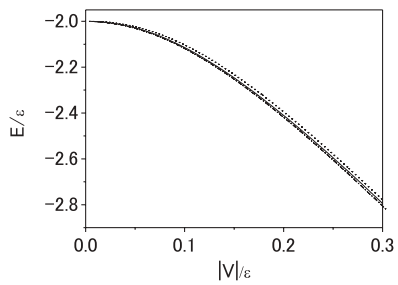

FIG. 4. Same as Fig. 3, but for $U = V$.

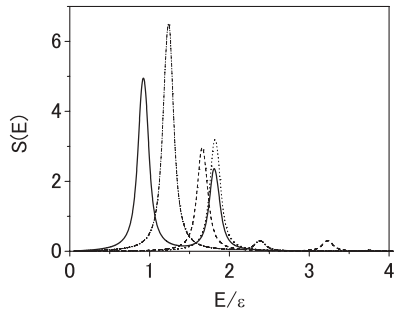

FIG. 5. Strength distributions of the one-phonon states calculated in STDDM (solid line), RPA (dotted line), and SRPA (dashed line) for $N = 4$ and $U/\epsilon = V/2\epsilon = -0.15$. The exact solution is shown with the dot-dashed line. The strength functions are smoothed with an artificial width $\Gamma_{\mathrm{FWHM}}/\epsilon = 0.125$.

Fig. 5. The first and third excited states in STDDM have strong mixing of two-body configurations, while the second excited state has relatively small mixing of two-body configurations.

For the exact solutions, the transition strength is split into four states. The fourth excited states have negligible strength, and the third excited states have some strength. In the case of $U = V$, the strength of the third excited state of the exact solution located at $E/\epsilon = 4.1$ is similar to that of the STDDM solution; while for $U = V/2$, the corresponding state located at $E/\epsilon = 3.8$ is invisible in the scale of Fig. 5.

In the case of $U = V/2$, the first excited state in STDDM has much larger transition strength than that in SRPA and has large collectivity comparable to the exact solution which also has strong mixing of two-phonon states. The difference in the first excited state between STDDM and SRPA seen in Fig. 5 demonstrates the importance of ground-state correlations, though it is not easy in our approach to clearly distinguish the various effects of ground-state correlations [16]. As far as the second excited state shown in Fig. 5 is concerned, however, STDDM (and also SRPA) poorly reproduces the excitation energy and transition strength. This problem might be understood by the fact that Eq. (6) does not properly describe two-phonon states: For example, self-energy terms for two-body configurations and also the coupling to three-phonon states are missing in Eq. (6) [12].

In the case of $U = V$ (Fig. 6) where the effects of ground-state correlations are small, the strength function in STDDM has better agreement with the exact one, while SRPA

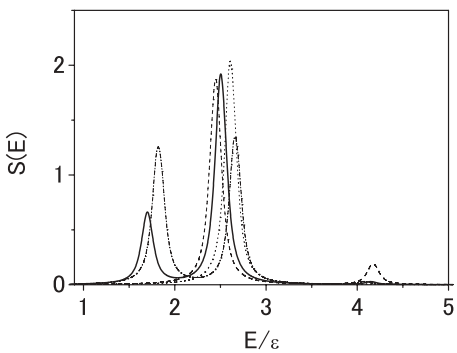

FIG. 6. Same as Fig. 5, but for $U/\epsilon = V/\epsilon = -0.3$.

cannot give the state corresponding to the first excited state of the exact solution. This indicates the importance of two-body configurations other than 2p-2h configurations considered in SRPA. Thus, it is found that STDDM can properly describe the fragmentation of a collective state in the extended Lipkin model, though a better treatment of two-phonon states may be required to reproduce the excitation energy and transition strength of each fragmented state.

B. Oxygen isotopes

1. Calculation details

Since the number of the two-body matrices $C_{\alpha\beta\alpha'\beta'}$ and $X^{\mu}_{\alpha\beta\alpha'\beta'}$ rapidly increases with increasing number of single-particle states, truncation of the single-particle space is necessary. Assuming that the single-particle states around the Fermi energy are most important for ground-state correlations, we use the four single-particle states, $1p_{3/2}$, $1p_{1/2}$, $1d_{5/2}$, and $2s_{1/2}$, for both protons and neutrons, to calculate $n_{\alpha\alpha'}$ and $C_{\alpha\beta\alpha'\beta'}$. The same single-particle states are used to define the two-body transition amplitude $X^{\mu}_{\alpha\beta\alpha'\beta'}$ in STDDM. In the case of ^{20}O and ^{22}O where the neutron $1d_{5/2}$ is occupied, a few more single-particle states are added to calculate $X^{\mu}_{\alpha\beta\alpha'\beta'}$ to investigate the effects of expansion of the single-particle space. To satisfy the energy-weighted sum rule, we use a large number of single-particle states for the one-body transition amplitude $x^{\mu}_{\alpha\alpha'}$. The continuum states are discretized by confining the single-particle wave functions in a sphere of radius 20 fm, and all single-particle states with $\epsilon_\alpha \leqslant 40$ MeV and orbital angular momentum $\ell \leqslant 4\hbar$ are taken. The effective interaction Skyrme III [19] is used to calculate single-particle energies and wave functions. To stabilize numerical calculations based on the gradient method, we replace the surface energy terms by the Yukawa interactions according to the same procedure as used in TDHF calculations [20]. Because of this replacement, the binding energies of the oxygen isotopes become slightly larger than the values obtained with the original Skyrme III. Since the calculation of matrix elements of the residual interaction is quite time consuming, we use a simple interaction derived from Skyrme III without the momentum-dependent terms,

$$\begin{aligned} v(\boldsymbol{r}-\boldsymbol{r}') &= t_0(1+x_0P_\sigma)\delta^3(\boldsymbol{r}-\boldsymbol{r}') \\ &\quad + \tfrac{1}{6}t_3(1+P_\sigma)\rho(\boldsymbol{r})\delta^3(\boldsymbol{r}-\boldsymbol{r}'), \end{aligned} \tag{11}$$

where P_σ is the spin exchange operator. A similar simple interaction has been used in recent QRPA calculations [21]. Since the residual interaction is different from Skyrme III which is used to calculate single-particle states, self-consistency is violated. As a consequence, the spurious mode associated with translational motion (isoscalar 1^- state) does not have zero energy in RPA. In fact, RPA with Eq. (11) gives pure imaginary energy solutions for the spurious mode. We decrease the strength of Eq. (11) using a renormalization factor f so that the spurious mode has approximately zero excitation energy in RPA. The factor depends on single-particle space and on nuclei. The values of the renormalization factor f_1 obtained for ^{16}O, ^{20}O, and ^{22}O are 0.62, 0.68, and 0.69, respectively. These values are used for the residual interaction in the matrix a in Eq. (6). Such a renormalization procedure using RPA may not be well defined for the residual interaction used in the matrix d which acts on the two-body space. An RPA calculation for the spurious mode in ^{16}O using the same single-particle states as used for $C_{\alpha\beta\alpha'\beta'}$ gives the normalization factor $f_2 = 0.99$. We use this value as a common renormalization factor of the residual interaction in matrix d for all the oxygen isotopes. The reduction factor to be used for matrices b and c are also not well determined. We use f_1 for matrices b and c. In ^{20}O, the excitation energy of the first 2^+ state (2^+_1) which mainly consists of a two neutron hole configuration of the $1d_{5/2}$ orbit, is sensitive to the residual interaction in the particle-particle channel; matrices b and d have such interaction terms. Since the residual interaction Eq. (11) does not give the correct excitation energy of 2^+_1, we slightly modify the particle-particle channel interaction for ^{20}O by reducing the value of x_0 from 0.45 to 0.3 and adding the following density-dependent interaction

$$v(\boldsymbol{r}-\boldsymbol{r}') = v_0(1-P_\sigma)(1-\rho(\boldsymbol{r})/\rho_0)\delta^3(\boldsymbol{r}-\boldsymbol{r}'), \tag{12}$$

which is commonly used in HFB calculations [4,21–24]. The values of v_0 and ρ_0 used are -150 MeV fm^3 and 0.16 fm^{-3}, respectively. The parameter v_0 is determined so that the experimental excitation energy (1.6 MeV) [25] of 2^+_1 in ^{20}O is reproduced in STDDM. The same modified interaction in the particle-particle channel is used also for ^{22}O. High-lying quadrupole states in ^{20}O and ^{22}O are little affected by this change in the particle-particle channel interaction. The HF ground state is used for ^{16}O as the starting ground state of the gradient method. The HF ground state where the neutron $1d_{5/2}$ is fully occupied is also used as the starting ground state of ^{22}O. In the case of ^{20}O, the two-hole state where the four last neutrons occupy the $1d_{5/2}$ is used as the starting ground state [13]. We consider only 2p-2h configurations for $C_{\alpha\beta\alpha'\beta'}$ and $X^{\mu}_{\alpha\beta\alpha'\beta'}$ and neglect two-body transition amplitudes whose excitation energies are greater than 40 MeV. In the case of ^{20}O, $C_{\alpha\beta\alpha'\beta'}$ and $X^{\mu}_{\alpha\beta\alpha'\beta'}$ where all single-particle indices are the neutron $1d_{5/2}$ orbit are also included to describe 2^+_1.

2. Ground states

The calculated occupation probabilities in ^{16}O are tabulated in Table I with the single-particle energies. The occupation probabilities largely deviate from the HF values, $n_{\alpha\alpha} = 1$ or 0, indicating strong mixing of 2p-2h configurations. Large

TABLE I. Single-particle energies ϵ_α and occupation probabilities $n_{\alpha\alpha}$ in ^{16}O.

Single-particle orbits	Protons		Neutrons	
	ϵ_α (MeV)	$n_{\alpha\alpha}$	ϵ_α (MeV)	$n_{\alpha\alpha}$
$1p_{3/2}$	−18.3	0.90	−21.9	0.90
$1p_{1/2}$	−12.3	0.88	−15.7	0.88
$1d_{5/2}$	−3.8	0.10	−7.1	0.10
$2s_{1/2}$	1.0	0.02	−1.5	0.02

TABLE II. Same as Table I, but for ^{20}O.

Single-particle orbits	Protons		Neutrons	
	ϵ_α (MeV)	$n_{\alpha\alpha}$	ϵ_α (MeV)	$n_{\alpha\alpha}$
$1p_{3/2}$	−25.7	0.97	−21.7	0.97
$1p_{1/2}$	−20.4	0.95	−16.6	0.97
$1d_{5/2}$	−11.1	0.03	−7.5	0.69
$2s_{1/2}$	−3.2	0.02	−2.2	0.03

mixing of 2p-2h configurations in the ground state of ^{16}O has been reported also by calculations in the shell model [26,27] and the generator coordinate method [28]. The calculated occupation probabilities do not agree with experimental observation, however. For example, proton knock out reactions ^{16}O$(e, e')^{15}$N suggest only 60% occupation of the $1p_{1/2}$ and $1p_{3/2}$ states and 2% occupation of the $1d_{5/2}$ and $2s_{1/2}$ states [29]. Such a discrepancy between measured occupation probabilities and calculated ones seems to be common for a wide range of nuclei [30]. To get an idea about the extent to which ground-state correlations contribute to the binding energy, we also calculate the total energy. The total energy $E_{\rm tot}$ in TDDM consists of the mean-field energy $E_{\rm MF}$ and the correlation energy $E_{\rm cor}$ defined by

$$E_{\rm MF} = \sum_{\alpha\alpha'} \langle \alpha' | t | \alpha \rangle n_{\alpha\alpha'} + \frac{1}{2} \sum_{\alpha\beta\alpha'\beta'} \langle \alpha'\beta' | v | \alpha\beta \rangle_A n_{\alpha\alpha'} n_{\beta\beta'}, \quad (13)$$

$$E_{\rm cor} = \frac{1}{2} \sum_{\alpha\beta\alpha'\beta'} \langle \alpha'\beta' | v | \alpha\beta \rangle C_{\alpha\beta\alpha'\beta'}, \quad (14)$$

where the subscript A means that the corresponding matrix is antisymmetrized. In ^{16}O, $E_{\rm tot} = E_{\rm MF} + E_{\rm cor} = -124.6\,{\rm MeV} - 23.8\,{\rm MeV} = -148.4\,{\rm MeV}$, while the starting HF energy $E_{\rm HF}$ is $-140.6\,{\rm MeV}$. The increase in $E_{\rm MF}$ due to the relaxation of the occupation probabilities from the HF values is largely compensated by the decrease in $E_{\rm cor}$.

The calculated occupation probabilities in ^{20}O and ^{22}O are tabulated in Tables II and III. The deviation of the occupation probabilities from the HF values in ^{20}O and ^{22}O is much smaller than that in ^{16}O, indicating weak ground-state correlations in these nuclei. The weak ground-state correlations in ^{20}O and ^{22}O may be explained by the occupation of the neutron $1d_{5/2}$ orbit which causes blocking of the 2p-2h transitions involving the neutron $1d_{5/2}$ state. Such blocking significantly reduces important proton-neutron correlations in the ground states of ^{20}O and ^{22}O. This interpretation may be justified by the fact that the deviation of $n_{\alpha\alpha}$ from the HF values in ^{20}O where the 2p-2h transitions involving the neutron $1d_{5/2}$ state is partially blocked is slightly larger than that in ^{22}O where such blocking is almost complete. To investigate the effects of truncation of the single-particle space on the ground-state correlations, we also performed a calculation for ^{22}O using two more single-particle states, that is, the proton and neutron $1d_{3/2}$ states, to define $n_{\alpha\alpha'}$ and $C_{\alpha\beta\alpha'\beta'}$ and found only a change of 0.003 $\sim$ 0.033 in the occupation numbers. The largest increase of 0.033 occurs in the occupation number of the neutron $1d_{3/2}$ state due to the transitions from the neutron $1p_{3/2}$ and $1p_{1/2}$ states. Thus, this calculation indicates that the weak ground-state correlations in ^{20}O and ^{22}O are not artifacts caused by the truncation of the single-particle space. The total energy in ^{20}O is $E_{\rm tot} = E_{\rm MF} + E_{\rm cor} = -160.7\,{\rm MeV} - 10.3\,{\rm MeV} = -171.0\,{\rm MeV}$, while $E_{\rm HF}$ is $-166.4\,{\rm MeV}$. In the case of ^{22}O, $E_{\rm tot} = E_{\rm MF} + E_{\rm cor} = -177.6\,{\rm MeV} - 4.4\,{\rm MeV} = -182.0\,{\rm MeV}$, and $E_{\rm HF}$ is $-180.0\,{\rm MeV}$. The correlation energy in ^{20}O is much larger than that in ^{22}O. This is because the pairing correlations originated in the neutron $[(1d_{5/2})^{-1} \times (1d_{5/2})^{-1}]$ configuration in ^{20}O. The difference in the binding energy between ^{20}O and ^{22}O is 11.0 MeV in TDDM, while it is 13.6 MeV in HF. The binding energy difference in TDDM is closer to the experimental value 10.6 MeV [25] than that in HF.

TABLE III. Same as Table I, but for ^{22}O.

Single-particle orbits	Protons		Neutrons	
	ϵ_α (MeV)	$n_{\alpha\alpha}$	ϵ_α (MeV)	$n_{\alpha\alpha}$
$1p_{3/2}$	−29.0	0.98	−21.8	0.995
$1p_{1/2}$	−24.0	0.97	−17.1	0.995
$1d_{5/2}$	−14.4	0.02	−7.8	0.998
$2s_{1/2}$	−5.7	0.01	−2.6	0.023

3. Quadrupole excitation

The strength functions for the quadrupole excitation in ^{16,20,22}O are shown in Figs. 7, 9, and 10. The excitation operator used is $r^2 Y_{20}(\theta)$. The strength functions are smoothed with an artificial width $\Gamma_{\rm FWHM} = 0.5$ MeV. The fraction of the energy-weighted sum-rule values depleted below 40 MeV in STDDM is 99% $\sim$ 102%. The energy-weighted sum rule is not completely satisfied because our calculations are not fully self-consistent. We first discuss the strength distribution in ^{16}O. The RPA (dotted line) gives GQR as a sharp resonance, similar to the result of the continuum RPA calculations [31]. SRPA (dot-dashed line) gives damping of GQR because 2p-2h configurations are mixed. However, the spreading of the strength is modest compared with the result in STDDM (solid line). In STDDM, a significant amount of strength is located below 15 MeV. This is consistent with experimental observation [32,33], which shows that the 2^+ states (except

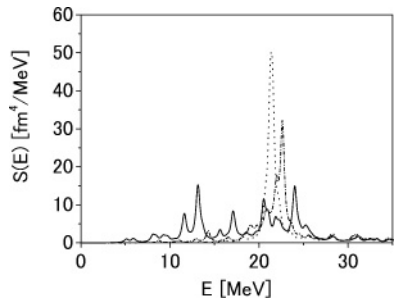

FIG. 7. Strength distributions of GQR in ^{16}O calculated in STDDM (solid line), RPA (dotted line), and SRPA (dot-dashed line). Strength functions are smoothed with an artificial width $\Gamma_{\rm FWHM} = 0.5$ MeV.

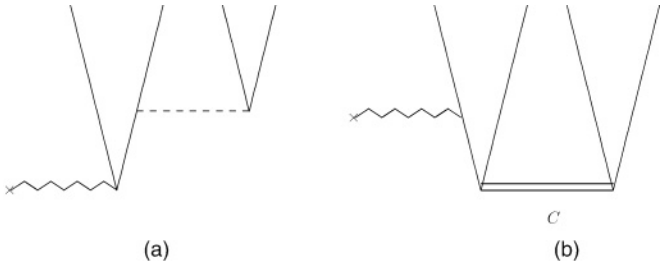

FIG. 8. (a) Damping process both in STDDM and SRPA. (b) Process only in STDDM. Wavy line means an external field (the quadrupole field in this case), dashed line is the interaction, and vertical lines indicate either particle states or hole states. The double line with C means $C_{\alpha\beta\alpha'\beta'}$.

for 2_1^+) below 18.5 MeV have 32% of the energy-weighted sum-rule value. The corresponding value in STDDM is 28%. Figure 8 shows coupling processes of a collective state consisting of p-h pairs to 2p-2h states. The wavy line denotes an external field (the quadrupole field in this case), the dashed line indicates the residual interaction, and the vertical lines mean either particle states or hole states. Figure 8(a) where a p-h pair is coupled to 2p-2h states is a damping process included in both SRPA and STDDM. Figure 8(b) represents one of the processes included only in STDDM where the external field is coupled to a 2p-2h configuration in the ground state. The peaks located in the region $10 < E < 15$ MeV is due to the process given by Fig. 8(b). In fact, these peaks become quite small when we neglect the terms corresponding to Fig. 8(b). The STDDM results demonstrate the importance of ground-state correlations in the large fragmentation of GQR. Main components of the peaks located in the region $10 < E < 15$ MeV are either $[1d_{5/2}(p)1d_{5/2}(n)(1p_{3/2}(p))^{-1}(1p_{1/2}(n))^{-1}]$ or $[1d_{5/2}(p)1d_{5/2}(n)(1p_{1/2}(p))^{-1}(1p_{3/2}(n))^{-1}]$, where (p) and (n) denote proton and neutron states, respectively. This means that proton-neutron correlations also play an important role in the splitting of GQR in ^{16}O. Shell-model calculations [34,35] also give large fragmentation of GQR in ^{16}O. However, the strength in the shell-model calculations is distributed in the region $E > 20$ MeV and the concentration of the strength in the region $10 < E < 15$ MeV is not reproduced. Some states are seen below 10 MeV in Fig. 7. Most of them consist of 1p-1h excitation from the partially occupied $1d_{5/2}$ states. These states could be components of the very collective 2_1^+. However, the description of 2_1^+ which is considered to be 4p-4h configurations [26,28] or an $\alpha+^{12}$C cluster state [36] is beyond the scope of our approach.

In the following, we discuss the quadrupole states in ^{20}O and ^{22}O shown in Figs. 9 and 10. The solid lines in Figs. 9 and 10 denote the results calculated using the proton and neutron $1p_{3/2}$, $1p_{1/2}$, $1d_{5/2}$, and $2s_{1/2}$ orbits for $X^{\mu}_{\alpha\beta\alpha'\beta'}$. The dotted lines depict the results in RPA and the dot-dashed lines indicate the results in STDDM obtained using a larger single-particle space as will be explained below. We first discuss 2_1^+. In RPA, the major component of 2_1^+ is the neutron-particle–hole configuration $[2s_{1/2}(n) \times (1d_{5/2}(n))^{-1}]$. STDDM gives much more collective 2_1^+ for ^{20}O than does RPA. This is due to mixing of the two-neutron–hole configuration

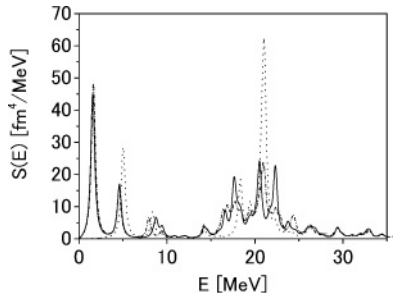

FIG. 9. Strength distributions of the quadrupole states in ^{20}O calculated in STDDM (solid line) and RPA (dotted line). Dot-dashed line depicts the STDDM result in which the neutron $1d_{3/2}$ and $2f_{7/2}$ states are added to define $X^{\mu}_{\alpha\beta\alpha'\beta'}$. Strength functions are smoothed with an artificial width $\Gamma_{\mathrm{FWHM}} = 0.5$ MeV.

$[(1d_{5/2}(n))^{-1} \times (1d_{5/2}(n))^{-1}]$ represented by $X^{\mu}_{\alpha\beta\alpha'\beta'}$. Thus, the pairing correlations which are usually treated using the pairing theories, HFB and QRPA, are taken into account also in STDDM. In fact, the TDDM-based approach has a close relation to HFB and QRPA as investigated in Ref. [37]. In the case of 2_1^+ in ^{22}O, STDDM gives a result similar to the RPA one except for a small energy shift due to the coupling to two-body configurations, reflecting the weak ground-state correlations in ^{22}O. The excitation energy of 2_1^+ in ^{22}O is 3.5 MeV, which is close to the experimental value of 3.2 MeV [38]. The $B(E2)$ values of 2_1^+ calculated in STDDM are $13e^2$ fm^4 in ^{20}O and $9e^2$ fm^4 in ^{22}O. These values are smaller than the experimental values of $28 \pm 2e^2$ fm^4 for ^{20}O [39] and $21 \pm 8e^2$ fm^4 for ^{22}O [40]. The $B(E2)$ values in STDDM sensitively depend on the strength of the residual interaction in the p-h channel and thus on the renormalization factor f_1, and it has also been pointed out [13] that the mixing of two-body configurations other than the 2p-2h configurations plays a role in enhancing the collectivity of 2_1^+ in ^{22}O. To obtain more reliable $B(E2)$ values for 2_1^+, therefore, we must perform self-consistent calculations using the same residual interaction as used for the mean-field potential and including more two-body configurations.

Now we discuss higher-lying quadrupole states. In the case of ^{20}O and ^{22}O, the strength functions in RPA show very

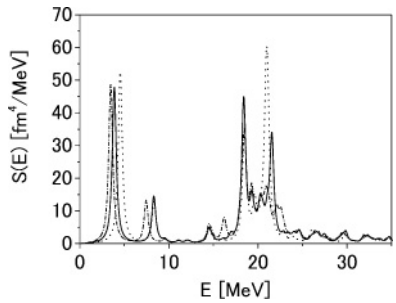

FIG. 10. Strength distributions of the quadrupole states in ^{22}O calculated in STDDM (solid line) and RPA (dotted line). Dot-dashed line depicts the STDDM result in which the proton and neutron $1d_{3/2}$ states and the neutron $2f_{7/2}$ state are added to calculate $X^{\mu}_{\alpha\beta\alpha'\beta'}$. Strength functions are smoothed with an artificial width $\Gamma_{\mathrm{FWHM}} = 0.5$ MeV.

fragmented distributions. The very collectives states in RPA located at 21.1 MeV in ^{20}O and 20.9 MeV in ^{22}O consist of both proton and neutron components and, therefore, correspond to GQR in ^{16}O. We call these states isoscalar modes [2]. Other states below 20 MeV are the so-called neutron modes mainly consisting of 1p-1h excitation from the neutron $1d_{5/2}$ orbit. The isoscalar modes are damped when 2p-2h configurations are mixed in STDDM, and the strength distribution becomes wider than that in RPA. However, the spreading of the quadrupole strength in ^{20}O and ^{22}O is not as large as that with GQR in ^{16}O. This may be explained by the blocking of 2p-2h configurations involving the neutron $1d_{5/2}$ state, as is the case of the ground states of these nuclei. This interpretation may be justified by the fact that the strength distribution in ^{20}O, where the blocking is imperfect, is wider than that in ^{22}O. The neutron modes in ^{22}O are little affected by the coupling to 2p-2h configurations. To show that the small damping of the quadrupole states in ^{20}O and ^{22}O are not artifacts due to the truncation of the single-particle space, we perform STDDM calculations (the dot-dashed lines in Figs. 9 and 10) using a few more single-particle states: for ^{20}O, the first $d_{3/2}$ ($1d_{3/2}$) and second $f_{7/2}$ ($2f_{7/2}$) neutron orbits are added to define $X^{\mu}_{\alpha\beta\alpha'\beta'}$; and for ^{22}O, the proton $1d_{3/2}$ state is also included in addition to the neutron $1d_{3/2}$ and $2f_{7/2}$ orbits. The reason that the neutron $2f_{7/2}$ orbit is included is that RPA calculations for negative-parity states (for example 3^- states) show strong coupling of the neutron $1d_{5/2}$ to the neutron $2f_{7/2}$ state. The first $f_{7/2}$ ($1f_{7/2}$) neutron orbit is unimportant in our calculation, because its small continuum energy makes the inner component of the wave function small. The proton $1d_{3/2}$ state is not included in ^{20}O, because the number of $X^{\mu}_{\alpha\beta\alpha'\beta'}$ is already quite large because of the partial occupation of the neutron $1d_{5/2}$ state. The number of $X^{\mu}_{\alpha\beta\alpha'\beta'}$ in the calculation shown by the dot-dashed line becomes 2.7 (5.7) times more in ^{20}O (in ^{22}O) than that shown by the solid line. As seen in Figs. 9 and 10, the increase of the number of single-particle states has only minor effects except for a slight energy shift of the state at $E = 8.3$ MeV in ^{22}O. To explain the difference in the damping property between the isoscalar modes and the neutron modes, we show in Fig. 11 the radial transition densities calculated in RPA for the neutron mode at $E = 18.5$ MeV and the isoscalar mode at $E = 20.9$ MeV in ^{22}O. Both transition densities have a peak at the nuclear surface. However, the transition density of the neutron mode has a smaller peak and a larger spatial extension

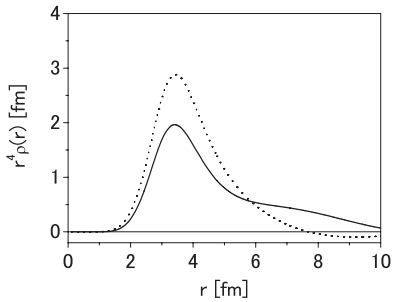

FIG. 11. Radial transition densities of the quadrupole states in ^{22}O at $E = 18.5$ MeV (solid line) and $E = 20.9$ MeV (dotted line) calculated in RPA.

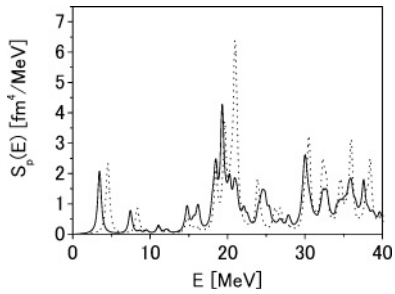

FIG. 12. Proton strength distributions of the quadrupole states in ^{22}O calculated in RPA (dotted line) and STDDM (solid line) with larger single-particle space corresponding to the dot-dashed line in Fig. 10. Strength functions for the excitation operator $r^2Y_{20}(\theta)$ are calculated using the proton components of the transition amplitudes. Strength functions are smoothed with an artificial width $\Gamma_{\rm FWHM} = 0.5$ MeV.

than that of the isoscalar mode. The small damping of the neutron mode may be explained by this large spatial extension of the transition density, which reduces the coupling to 2p-2h configurations. To get an idea about proton quadrupole excitation, we show in Fig. 12 the proton strength function for ^{22}O. The solid line depicts the large space STDDM calculation corresponding to the result indicated by the dot-dashed line in Fig. 10. The strength distribution above 25 MeV corresponds to the components of the isovector quadrupole resonance. The damping of the isoscalar mode and the isovector components are seen in Fig. 12.

IV. SUMMARY

Applications of an extended version of the Hartree-Fock theory (HF) and the random-phase approximation (RPA) derived from the time-dependent density-matrix theory (TDDM) were presented. In this TDDM-based formalism, the ground state is given as a stationary solution of the TDDM equations, and excited states are calculated using the small-amplitude limit of TDDM (STDDM). The first application was to an extended version of the Lipkin model designed to include the damping of a one-phonon state. It was found that the ground-state energies calculated in TDDM agree quite well with the exact values, and that STDDM properly describes the damping of a one-phonon state. As realistic applications, the ground states and the quadrupole states including giant quadrupole resonances (GQRs) of the oxygen isotopes ^{16,20,22}O were calculated. It was found that ^{16}O has stronger ground-state correlations than ^{20}O and ^{22}O. It was also found that GQR in ^{16}O has a much larger spreading width than the corresponding quadrupole states in ^{20}O and ^{22}O. It was pointed out that the neutron modes have small damping effects. It was discussed that the occupation of the neutron $1d_{5/2}$ state in ^{20}O and ^{22}O is responsible for the weak ground-state correlations and for the small damping of the quadrupole states in these nuclei. The obtained results demonstrate that the TDDM-based approach gives a much more realistic description of nuclear collective excitation than do the RPA and QRPA approaches. However, a self-consistent treatment of the residual interaction is required to obtain more quantitative results.

APPENDIX

Matrices a, b, c, and d are shown below. The single-particle states are given by $h\phi_\alpha = \epsilon_\alpha \phi_\alpha$, where h is the mean-field Hamiltonian.

$$a(\alpha\alpha' : \lambda\lambda') = (\epsilon_\alpha - \epsilon_{\alpha'})\delta_{\alpha\lambda}\delta_{\alpha'\lambda'} - \sum_\beta (\langle\beta\lambda'|v|\alpha'\lambda\rangle_A n_{\alpha\beta} - \langle\alpha\lambda'|v|\beta\lambda\rangle_A n_{\beta\alpha'}), \tag{A1}$$

$$\begin{aligned}
&b(\alpha_1\alpha_2\alpha_1'\alpha_2' : \lambda\lambda') \\
&= -\delta_{\alpha_1\lambda}\Bigg\{\sum_{\beta\gamma\delta}\big[\big(\delta_{\alpha_2\beta} - n_{\alpha_2\beta}\big)n_{\gamma\alpha_1'}n_{\delta\alpha_2'} \\
&\quad + n_{\alpha_2\beta}\big(\delta_{\gamma\alpha_1'} - n_{\gamma\alpha_1'}\big)\big(\delta_{\delta\alpha_2'} - n_{\delta\alpha_2'}\big)\big] \\
&\quad \times \langle\lambda'\beta|v|\gamma\delta\rangle_A + \sum_{\beta\gamma}\big[\langle\lambda'\alpha_2|v|\beta\gamma\rangle \\
&\quad \times C_{\beta\gamma\alpha_2'\alpha_2'} + \langle\lambda'\beta|v|\alpha_1'\gamma\rangle_A C_{\alpha_2\gamma\alpha_2'\beta} \\
&\quad - \langle\lambda'\beta|v|\alpha_2'\gamma\rangle_A C_{\alpha_2\gamma\alpha_1'\beta}\big]\Bigg\} + \delta_{\alpha_2\lambda} \\
&\quad \times \Bigg\{\sum_{\beta\gamma\delta}\big[\big(\delta_{\alpha_1\beta} - n_{\alpha_1\beta}\big)n_{\gamma\alpha_1'}n_{\delta\alpha_2'} + n_{\alpha_1\beta}\big(\delta_{\gamma\alpha_1'} - n_{\gamma\alpha_1'}\big) \\
&\quad \times \big(\delta_{\delta\alpha_2'} - n_{\delta\alpha_2'}\big)\big]\langle\lambda'\beta|v|\gamma\delta\rangle_A \\
&\quad + \sum_{\beta\gamma}\big[\langle\lambda'\alpha_1|v|\beta\gamma\rangle C_{\beta\gamma\alpha_1'\alpha_2'} + \langle\lambda'\beta|v|\alpha_1'\gamma\rangle_A C_{\alpha_1\gamma\alpha_2'\beta} \\
&\quad - \langle\lambda'\beta|v|\alpha_2'\gamma\rangle_A C_{\alpha_1\gamma\alpha_1'\beta}\big]\Bigg\} + \delta_{\alpha_1'\lambda'}\Bigg\{\sum_{\beta\gamma\delta}\big[\big(\delta_{\delta\alpha_2'} - n_{\delta\alpha_2'}\big) \\
&\quad \times n_{\alpha_1\beta}n_{\alpha_2\gamma} + n_{\delta\alpha_2'}\big(\delta_{\alpha_1\beta} - n_{\alpha_1\beta}\big)\big(\delta_{\alpha_2\gamma} - n_{\alpha_2\gamma}\big)\big] \\
&\quad \times \langle\beta\gamma|v|\lambda\delta\rangle_A + \sum_{\beta\gamma}\big[\langle\beta\gamma|v|\lambda\alpha_2'\rangle C_{\alpha_1\alpha_2\beta\gamma} \\
&\quad + \langle\alpha_1\beta|v|\lambda\gamma\rangle_A C_{\alpha_2\gamma\alpha_2'\beta} - \langle\alpha_2\beta|v|\lambda\gamma\rangle_A C_{\alpha_1\gamma\alpha_2'\beta}\big]\Bigg\} \\
&\quad - \delta_{\alpha_2'\lambda'}\Bigg\{\sum_{\beta\gamma\delta}\big[\big(\delta_{\delta\alpha_1'} - n_{\delta\alpha_1'}\big)n_{\alpha_1\beta}n_{\alpha_2\gamma} + n_{\delta\alpha_1'} \\
&\quad \times \big(\delta_{\alpha_1\beta} - n_{\alpha_1\beta}\big)\big(\delta_{\alpha_2\gamma} - n_{\alpha_2\gamma}\big)\big]\langle\beta\gamma|v|\lambda\delta\rangle_A \\
&\quad + \sum_{\beta\gamma}\big[\langle\beta\gamma|v|\lambda\alpha_1'\rangle C_{\alpha_1\alpha_2\beta\gamma} + \langle\alpha_1\beta|v|\lambda\gamma\rangle_A \\
&\quad \times C_{\alpha_2\gamma\alpha_1'\beta} - \langle\alpha_2\beta|v|\lambda\gamma\rangle_A C_{\alpha_1\gamma\alpha_1'\beta}\big]\Bigg\} \\
&\quad + \sum_\beta\big[\langle\alpha_1\lambda'|v|\beta\lambda\rangle_A C_{\beta\alpha_2\alpha_1'\alpha_2'} - \langle\alpha_2\lambda'|v|\beta\lambda\rangle_A \\
&\quad \times C_{\beta\alpha_1\alpha_1'\alpha_2'} - \langle\beta\lambda'|v|\alpha_2'\lambda\rangle_A C_{\alpha_1\alpha_2\alpha_1'\beta} \\
&\quad + \langle\beta\lambda'|v|\alpha_1'\lambda\rangle_A C_{\alpha_1\alpha_2\alpha_2'\beta}\big],
\end{aligned} \tag{A2}$$

$$c(\alpha\alpha' : \lambda_1\lambda_2\lambda_1'\lambda_2') = \langle\alpha\lambda_2'|v|\lambda_1\lambda_2\rangle\delta_{\alpha'\lambda_1'} - \langle\lambda_1'\lambda_2'|v|\alpha'\lambda_2\rangle\delta_{\alpha\lambda_1}, \tag{A3}$$

$$\begin{aligned}
&d(\alpha_1\alpha_2\alpha_1'\alpha_2' : \lambda_1\lambda_2\lambda_1'\lambda_2') \\
&\quad = \big(\epsilon_{\alpha_1} + \epsilon_{\alpha_2} - \epsilon_{\alpha_1'} - \epsilon_{\alpha_2'}\big)\delta_{\alpha_1\lambda_1}\delta_{\alpha_2\lambda_2}\delta_{\alpha_1'\lambda_1'}\delta_{\alpha_2'\lambda_2'} \\
&\quad + \delta_{\alpha_1'\lambda_1'}\delta_{\alpha_2'\lambda_2'}\sum_{\beta\gamma}\big(\delta_{\alpha_1\beta}\delta_{\alpha_2\gamma} - \delta_{\alpha_2\gamma}n_{\alpha_1\beta} - \delta_{\alpha_1\beta}n_{\alpha_2\gamma}\big) \\
&\quad \times \langle\beta\gamma|v|\lambda_1\lambda_2\rangle - \delta_{\alpha_1\lambda_1}\delta_{\alpha_2\lambda_2}\sum_{\beta\gamma}\big(\delta_{\alpha_1'\beta}\delta_{\alpha_2'\gamma} \\
&\quad - \delta_{\alpha_2'\gamma}n_{\alpha_1'\beta} - \delta_{\alpha_1'\beta}n_{\alpha_2'\gamma}\big)\langle\lambda_1'\lambda_2'|v|\beta\gamma\rangle + \delta_{\alpha_2\lambda_2}\delta_{\alpha_2'\lambda_2'} \\
&\quad \times \sum_\beta\big(\langle\alpha_1\lambda_1'|v|\beta\lambda_1\rangle_A n_{\beta\alpha_1'} - \langle\beta\lambda_1'|v|\alpha_1'\lambda_1\rangle_A n_{\alpha_1\beta}\big) \\
&\quad + \delta_{\alpha_2\lambda_2}\delta_{\alpha_1'\lambda_1'}\sum_\beta\big(\langle\alpha_1\lambda_2'|v|\beta\lambda_1\rangle_A n_{\beta\alpha_2'} \\
&\quad - \langle\beta\lambda_2'|v|\alpha_2'\lambda_1\rangle_A n_{\alpha_1\beta}\big) + \delta_{\alpha_1\lambda_1}\delta_{\alpha_1'\lambda_1'} \\
&\quad \times \sum_\beta\big(\langle\alpha_2\lambda_2'|v|\beta\lambda_2\rangle_A n_{\beta\alpha_2'} - \langle\beta\lambda_2'|v|\alpha_2'\lambda_2\rangle_A n_{\alpha_2\beta}\big) \\
&\quad + \delta_{\alpha_1\lambda_1}\delta_{\alpha_2'\lambda_2'}\sum_\beta(\langle\alpha_2\lambda_1'|v|\beta\lambda_2\rangle_A n_{\beta\alpha_1'} \\
&\quad - \langle\beta\lambda_1'|v|\alpha_1'\lambda_2\rangle_A n_{\alpha_2\beta}).
\end{aligned} \tag{A4}$$

[1] P. Ring and P. Schuck, *The Nuclear Many-Body Problem* (Springer, Berlin, 1980) and references therein.
[2] M. Yokoyama, T. Otsuka, and N. Fukunishi, Phys. Rev. C **52**, 1122 (1995).
[3] H. Sagawa and H. Esbensen, Nucl. Phys. **A693**, 448 (2001).
[4] E. Khan, N. Sandulescu, M. Grasso, and N. V. Giai, Phys. Rev. C **66**, 024309 (2002).
[5] J. Terasaki, J. Engel, M. Bender, J. Dobaczewski, W. Nazarewicz, and M. Stoitsov, Phys. Rev. C **71**, 034310 (2005).
[6] S. Drożdż, S. Nishizaki, J. Speth, and J. Wambach, Phys. Rep. **197**, 1 (1990) and references therein.
[7] S. J. Wang and W. Cassing, Ann. Phys. (NY) **159**, 328 (1985); W. Cassing and S. J. Wang, Z. Phys. A **328**, 423 (1987).
[8] M. Gong and M. Tohyama, Z. Phys. A **335**, 153 (1990).
[9] M. Tohyama and M. Gong, Z. Phys. A **332**, 269 (1989).
[10] M. Tohyama, Prog. Theor. Phys. **92**, 905 (1994).
[11] M. Tohyama, S. Takahara, and P. Schuck, Eur. Phys. J. A **21**, 217 (2004).

[12] S. Takahara, M. Tohyama, and P. Schuck, Phys. Rev. C **70**, 057307 (2004).
[13] M. Tohyama, Prog. Theor. Phys. **114**, 1021 (2005).
[14] H. J. Lipkin, N. Meshkov, and A. J. Glick, Nucl. Phys. **62**, 188 (1965).
[15] M. Tohyama and P. Schuck, Eur. Phys. J. A **19**, 215 (2004).
[16] K. Takayanagi, K. Shimizu, and A. Arima, Nucl. Phys. **A477**, 205 (1988).
[17] D. Shindo and K. Takayanagi, Phys. Rev. C **68**, 014312 (2003).
[18] S. T. Yang, J. Heyer, and T. T. S. Kuo, Nucl. Phys. **A448**, 420 (1986).
[19] M. Beiner, H. Flocard, Ngyen Van Giai, and P. Quentin, Nucl. Phys. **A238**, 29 (1975).
[20] K. T. R. Davies and S. E. Koonin, Phys. Rev. C **23**, 2042 (1981).
[21] M. Matsuo, Nucl. Phys. **A696**, 371 (2001).
[22] R. R. Chasman, Phys. Rev. C **14**, 1935 (1976).
[23] J. Terasaki, H. Flocard, P.-H. Heenen, P. Bonche, Nucl. Phys. **A621**, 706 (1997).
[24] N. Yamagami and Nguyen Van Giai, Phys. Rev. C **69**, 034301 (2004).
[25] R. B. Firestone, V. S. Shirley, C. M. Baglin, S. Y. F. Chu, and J. Zipkin, *Table of Isotopes, 8th ed.* (John Wiley & Sons, New York, 1996).
[26] W. C. Haxton and C. Johnson, Phys. Rev. Lett. **65**, 1325 (1990).
[27] E. K. Warburton, B. A. Brown, and D. J. Millener, Phys. Lett. **B293**, 7 (1992).
[28] M. Bender and P.-H. Heenen, Nucl. Phys. **A713**, 390 (2003).
[29] M. Leuschner, J. R. Calarco, F. W. Hersman, E. Jans, G. J. Kramer, L. Lapikás, G. van der Steenhoven, P. K. A. de Witt Huberts, H. P. Blok, N. Kalantar-Nayestanaki, and J. Friedrich, Phys. Rev. C **49**, 955 (1994).
[30] J. Lee, J. A. Tostevin, B. A. Brown, F. Delaunay, W. G. Lynch, M. J. Saelim, and M. B. Tsang, Phys. Rev. C **73**, 044608 (2006).
[31] G. F. Bertsch and S. F. Tsai, Phys. Rep. **C18**, 125 (1975).
[32] A. Hotta, K. Itoh, and T. Saito, Phys. Rev. Lett. **33**, 790 (1974).
[33] K. T. Knöpfle, G. J. Wagner, H. Breuer, M. Rogge, and C. Mayer-Böricke, Phys. Rev. Lett. **35**, 779 (1975).
[34] T. Hoshino and A. Arima, Phys. Rev. Lett. **37**, 266 (1976).
[35] T. Hoshino, H. Sagawa, and A. Arima, Nucl. Phys. **A481**, 458 (1988).
[36] Y. Suzuki and S. Hara, Phys. Rev. C **39**, 658 (1989).
[37] M. Tohyama and S. Takahara, Prog. Theor. Phys. **112**, 499 (2004).
[38] M. Belleguic, M. J. Lòpez-Jiménez, M. Stanoiu, F. Azaiez, M.-G. Saint-Laurent, O. Sorlin, N. L. Achouri, J.-C. Angélique, C. Bourgeois, C. Borcea, J.-M. Daugas, C. Donzaud, F. De Oliveira-Santos, J. Duprat, S. Grévy, D. Guillemaud-Mueller, S. Leenhardt, M. Lewitowicz, Yu.-E. Penionzhkevich, and Yu. Sobolev, Nucl. Phys. **A682**, 136c (2001).
[39] S. Raman, C. H. Malarkey, W. T. Milner, C. W. Nestor, Jr., and P. H. Stelson, At. Data Nucl. Data Tables **36**, 1 (1987).
[40] P. G. Thirolf, B. V. Pritychenko, B. A. Brown, P. D. Cottle, M. Chromik, T. Glasmacher, G. Hackman, R. W. Ibbotson, K. W. Kemper, T. Otsuka, L. A. Riley, and H. Scheit, Phys. Lett. **B485**, 16 (2000).